Journal of Building Engineering 35 (2021) 102050

Contents lists available at ScienceDirect

Journal of Building Engineering

journal homepage: http://www.elsevier.com/locate/jobe

Combining Kriging meta models with U-function and K-Means clustering for prediction of fracture energy of concrete

Iman Afshoon, Mahmoud Miri *, Seyed Roohollah Mousavi

Civil Engineering Department, University of Sistan and Baluchestan, Zahedan, Iran

ARTICLE INFO

Keywords:
Fracture energy
Prediction model
Concrete
Kriging method
U-learning function
K-means clustering

ABSTRACT

In this study, a combination of Kriging surrogate method with U-learning function and K-means clustering were used to predict the concrete fracture energy (as an output parameter) based on previous experimental data sets including compressive strength, maximum aggregate size and the water to cement ratio (as the input parameters). Therefore a collection of 246 data series obtained from previous studies was collected. The strength, accuracy, and efficiency of the proposed models were examined by selecting 10%, 30%, and 50% of the data for learning, and the results were compared with the previous equations. The results show that combining the Kriging method with the U-learning function in the work of fracture method (WFM) will increase the predictive power of fracture energy compared to basic Kriging and K-means clustering methods, and the previous relationships. However, the size effect method (SEM), the models created using K-means and 50% of the data has led to better forecasting results than other models. The value of the correlation coefficient (R^2) of the proposed Kriging combination models and previous existing relationships are in the range of 0.59–0.95 and 0.14–0.69, respectively. The results show that the combination of the Kriging method, the U-learning function, and K-means clustering will reduce the time and cost of the experiments, as well as increasing the accuracy of concrete fracture energy prediction results using a small number of previous experimental data.

1. Introduction

The growth and expansion of micro-cracks and their transformation into large and continuous cracks will lead to the fracture of concrete [1]. Investigating the solutions to prevent and control the growth of micro-cracks in concrete elements increases safety and reduces the economic losses and casualties caused by the fracture and collapse [2]. As micro-cracks cover a large area and prevent the rapid expansion of cracks, structural engineers consider the size effect parameter (fracture energy (G_f) (initial fracture energy)) to examine the impact of the member's dimensions on its ultimate strength [3]. Therefore, when the purpose is to examine the performance of the real elements using small-scale samples in a laboratory, the significance of the size effect concept becomes more apparent. In addition, the classification of materials (brittle, quasi-brittle, and elastic-plastic) and the determination of their linear or nonlinear performance in structures are based on the size and recognition of the fracture process zone (FPZ) at the end of the crack [4,5]. To study the fracture parameters of different materials, use can be made of the size effect method [4,6], work fracture method [4,7], crack band method [8], effective crack method [9], two parameter model [10], cohesive crack method or fictitious crack method [11,12], double-G fracture method [13], KR-curve method [14,15], double-K fracture method [16–19], boundary effect method and simplified boundary effect method [20,21].

In calculating the size effect fracture energy (G_f), the test specimens have the same geometry (shape), but vary in size. For this reason, the fracture energy calculated in size effect method (SEM) does not depend on the size, shape and geometry of the samples. As the maximum applied load and the area under the load-displacement graph before the maximum load is used to calculate the G_f, it is called the initial fracture energy (Fig. 1) [5]. Another method used to study the fracture energy is called work fracture method (WFM). In this method, the specific fracture energy (G_F) is the same energy used to create the unit area of crack. Conventional-sized samples are used in WFM to calculate the G_F, and the amount of the fracture energy depends entirely on the size and shape of the samples. In this method the fracture energy will be calculated by calculating the total area under the load-displacement diagram (Fig. 1), [5].

* Corresponding author.
E-mail address: mmiri@eng.usb.ac.ir (M. Miri).

https://doi.org/10.1016/j.jobe.2020.102050
Received 15 August 2020; Received in revised form 20 November 2020; Accepted 28 November 2020
Available online 2 December 2020

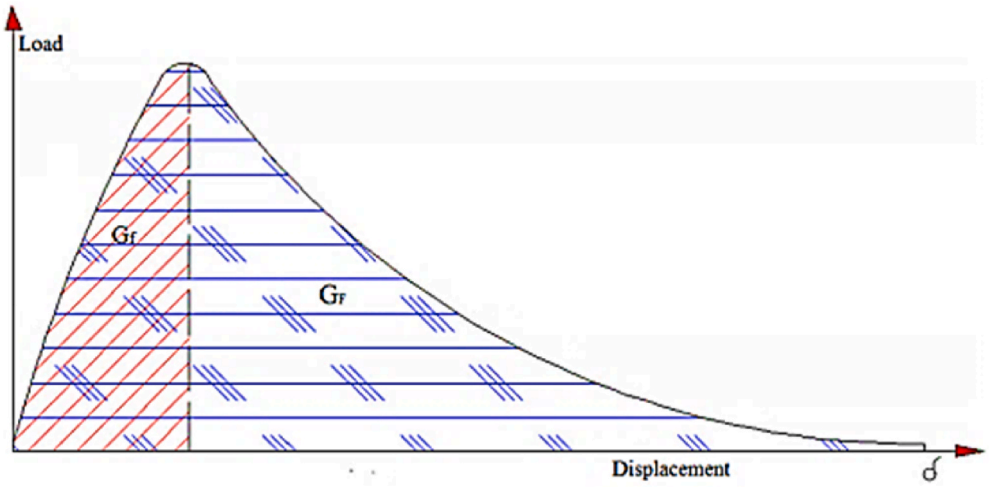

Fig. 1. G_f and G_F in the load-displacement curve [50].

The fracture energy in WFM is always greater than the fracture energy obtained from SEM [22,23]. There are different points of view to the existence or non-existence of a clear relationship between these two parameters [24,25]. This difference is caused by various reasons such as the size and shape of the samples, how the experiments were performed, the distribution and the uncertainty of the fracture energy values obtained from the WFM after the maximum load and in the final part of the load-displacement diagram compared to the SEM fracture energy [4, 23]. Bazant and Becq-giradun [24] reported a value of about 2.5 for the G_F/G_f in typical concrete. While Beygi et al. [10] claimed that for self-compacting concrete (SCC), this ratio is 3.11. Ghasemi et al. [27] reported G_F/G_f ratio for SCC with steel fibers to be 9.66. Researches by Kazemi et al. [28] showed that in high-strength concrete with steel fibers, the G_F/G_f value is approximately equal to 10.5. The WFM method yields better fracture energy results than SEM because it considers the total area under the load-displacement diagram and the post cracking behavior of concrete [4]. Furthermore, the physical sample size is not adequate to describe the size effect on the fracture properties observed on laboratory-size samples because depending on the relationship between the sample width and the ligament transition length, a boundary effect and the size effect can exist [21].

Water-to-cement ratio (W/C), aggregate properties, amount and characteristics of admixtures, etc. are among the parameters affecting crack propagation and accelerating the fracture phenomenon in concrete [29]. According to research by Wittmann et al. [30], increasing the W/C in conventional concrete reduces the fracture energy. Carpinteri and Brighenti [31] reported that using the optimal amount of W/C generates the maximum fracture energy due to increased quality and strength of cement paste, especially in the area of contact with aggregates. They believed that this happens because the high strength of the cement paste almost prevents the spread of micro-cracks in this area. According to the studies by Nallathambi et al. [32], when the amount of W/C is high, the expansion and growth of cracks occurs more rapidly. Previous studies reported a decrease in fracture energy when W/C is too low or too high [26]. However, some researchers have presented different results on the relationship between W/C ratio and fracture parameters. For example, Mindess et al. [33] and Phillips and Binsheng [34] reported that the fracture energy does not change with increasing or decreasing the W/C ratio. According to Zhao et al. [35], there is no clear and tangible relationship between these two parameters. However, Ince and Alyamac [36] used Abrams' law to confirm the existence of a specific relationship between W/C ratio and fracture characteristics.

Aggregates make up more than 70% of the concrete volume. For this reason, the performance and behavior of concrete at different ages are strongly influenced by the properties of these materials [37]. Although there is no specific relationship between the size of the aggregate and fracture toughness [38], increasing the amount and maximum size of aggregates (d_{max}) will have a positive effect on the failure properties [39,40]. Many researchers have reported that increasing the maximum size of the aggregates increases the fracture energy of concrete [41–43]. The studies by Petersson [44] showed that improving the quality and strength of the aggregates will have a positive effect on the fracture characteristics. Ince and Alyamac [36] reported that when the compressive strength of typical concrete (normal vibrating concrete) increases, the characteristics of the failure phenomenon such as energy and toughness increase. Compressive strength plays an important role in increasing fracture energy and toughness of high strength concretes. Although increasing the maximum size of the aggregates in this type of concrete will increase the compressive strength, unlike ordinary concretes, the failure energy of high-strength concretes is more affected by the type of aggregates [32–34].

Providing prediction models that have the desired strength, accuracy, and low cost to estimate the various parameters of materials, based on existing experimental input and output data sets, has always been interesting for researchers. In addition to multiple linear regressions, artificial intelligence methods such as artificial neural networks (ANN), adaptive neuro-fuzzy inference systems (ANFIS), and fuzzy and neuro-fuzzy systems have been used to estimate the complex performance of the structural materials [23,45,46]. Some Meta models such as Kriging surrogate, response surface methodology, dimension reduction prediction, etc. have also been used for this purpose [47–49]. Because concrete falls into the category of quasi-brittle materials and has a complex nonlinear behavior in fracture, assessment and obtaining an accurate fracture behavior model for this material play a key role in for an ideal, optimal, and safe design. Due to the cost and time reduction, it is very useful to provide an accurate model of failure behavior using existing experimental data sets and based on prediction methods and formulas [23].

2. Significance of the study

Investigating the concrete characteristics requires time, money, designs of experiments (DoE), preparation of materials and testing with special equipment at the desired ages. Therefore, the use of solutions that prevents or reduces the loss of cost, time and other disadvantages is needed in the concrete industry. In addition, human error due to the lack of skills and adequate knowledge of basic theories, the poor performance of the researcher during the experiment and equipment errors such as

Table 1
Existing relationships for fracture energy prediction of concrete.

Ref.	Equation	detail
Bazant and Becq-Giraudon [56]	$G_f = a_0\left(f_c/0.051\right)^{0.46}\left(1+d_{max}/11.27\right)^{0.22}\left(w/c\right)^{-0.3}$ $G_F = 2.5G_f$	G_f = fracture energy of SEM $\left(N/m\right)$ G_F = fracture energy of WFM $\left(N/m\right)$ f_c = cylinder compressive strength(MPa) d_{max} = maximum aggregate size(mm) $\frac{w}{c}$ = water to cement ratio $a_0 = 1$ for rounded aggregate $a_0 = 1.44$ for crushed aggregate
CEB-90 [57]	$G_F = (0.0469d_{max}^2 - 0.5d_{max} + 26)\left(f_c/10\right)^{0.7}$	G_F = fracture energy of WFM $\left(N/m\right)$ f_c = cylinder compressive strength(MPa) d_{max} = maximum aggregate size(mm)
CEB-2010 [58]	$G_F = 73(f_{cm})^{0.18}$ $f_{cm} = f_{ck} + 8$	G_F = fracture energy of WFM $\left(N/m\right)$ f_{cm} = mean value of cylinder compressive strength(MPa) f_{ck} = specific characteristic compressive strength(MPa)
JSCE [59]	$G_F = 10(d_{max})^{0.33}(f_c)^{0.33}$	G_F = fracture energy of WFM $\left(N/m\right)$ f_c = cylinder compressive strength(MPa) d_{max} = maximum aggregate size(mm)

lack of proper calibration or burnout will lead to a waste of time and money and also unreliable results. On the other hand, it may not be possible to perform the test due to the lack of special equipment and devices [23]. Therefore, it is very useful to use prediction models to determine the parameters of concrete fracture based on available experimental data. The use of regression-based methods, presented in codes and researches as experimental formulas, cannot accurately describe the complex and nonlinear nature of the mechanical properties of concrete, especially the fracture energy, based on previous experimental data sets [23]. For this reason, the use of regression-based relationships cannot fully ensure the user's satisfaction in predicting the fracture parameters [51]. The use of statistical analysis and prediction models to estimate the concrete fracture parameters based on experimental data sets has been investigated by many researchers [36–55].

An estimation method with a high accuracy and less required initial data set is needed to extract the target function. Among surrogate methods, the Kriging method is efficient in problems with a high nonlinearity [48]. This is due to the possibility of creating a predictive model that has sufficient power to detect the input and output relationships between data sets by introducing several points of DoE. In general, the selection, finding the appropriate number and the definition process of these points by using existing data sets is not easy. In this study, a database of 246 data sets was prepared including three input parameters (compressive strength, maximum aggregate diameter, and water to cement ratio) and one output parameter (fracture energy). Then, by combining the Kriging method with the U-learning function and K-means clustering and selecting 10%, 30%, and 50% of the available data as design points (learning data), different models of fracture energy assessment of concrete are examined. Finally, the results and errors of the proposed models are compared with previous relationships.

3. Existing relationships to predict concrete fracture energy

Various equations and relationships have been proposed in recent decades to estimate the fracture energy of typical concrete using regression and the experimental samples. Some of these equations that have been used by researchers and codes are shown in Table 1. These relationships, which are often based on statistics and regression, are not accurate enough. Therefore surrogate methods are needed for more accurate assessments.

4. Kriging method

The original idea for the Kriging surrogate was developed by Daniel Krige and very fast became a common method as a low-cost simulation approach [60]. Kriging method is widely used in reliability assessment and collapse probability problems. Compared to the other surrogate methods, this method is known as an accurate interpolation method and the design points predicted by this method are exactly the same as the actual output values. The user can also increase the prediction accuracy of the Kriging model to the desired level by adding new design points to the basic design point sets [61–64].

By considering the $G(\boldsymbol{x})$ response function the basic Kriging model is created (Eq. (1)). $G(\boldsymbol{x})$ consists of two parts and in this equation, the first part, $F(\boldsymbol{x}.\boldsymbol{\beta})$ and the second part, $Z(\boldsymbol{x})$, are the regression model and the stochastic process, respectively [61,65,66]:

$$G(\boldsymbol{x}) = F(\boldsymbol{x}.\boldsymbol{\beta}) + Z(\boldsymbol{x}) = \mathbf{f}(\boldsymbol{x})^T\boldsymbol{\beta} + Z(\boldsymbol{x}) \quad (1)$$

where $\mathbf{f}(\boldsymbol{x})^T = [\mathrm{f}_1(\boldsymbol{x}).\mathrm{f}_2(\boldsymbol{x}).....\mathrm{f}_m(\boldsymbol{x})]^T$ and $\boldsymbol{\beta}^T = [\beta_1.\beta_2.....\beta_m]^T$ are basic function and corresponding regression coefficient, respectively.$F(\boldsymbol{x}.\boldsymbol{\beta}) = F(\boldsymbol{x}.\beta) + Z(\boldsymbol{x})$ is the Gaussian function with an average value of zero. Covariance will be presented as Eq. (2).

$$Cov(p.r) = \sigma^2 R(\theta.\boldsymbol{p}.\boldsymbol{r}) \quad (2)$$

where σ^2 and $R(\theta.\boldsymbol{p}.\boldsymbol{r})$ are process variance and Gaussian correlation function between $\boldsymbol{p}$ and $\boldsymbol{r}$ points selected with the θ parameter, respectively. In this study, the Gaussian correlation function is used according to Eq. (3).

$$R(\theta.\boldsymbol{p}.\boldsymbol{r}) = \prod_{j=1}^{c}\exp\left[-\theta_j\left(p_j - r_j\right)^2\right] \quad (3)$$

where p_j and r_j are the j-th member of the $\boldsymbol{p}$ and $\boldsymbol{r}$ points vectors, respectively and θ_j is a scalar that expresses the multiplicative inverse of the correlation length in the j-th direction. $\boldsymbol{x} = [\boldsymbol{x}^{(1)}.\boldsymbol{x}^{(2)}.....\boldsymbol{x}^{(n)}]$is the design points set in which $\boldsymbol{x}^{(i)}$is the ith design point (leaning data) and $\boldsymbol{y} = [y_1.y_2.....y_n]$ is the corresponding response provided using test

Table 2
Description of experimental datasets.

Ref.	Specimens Number	f_c (MPa)	d_{max} (mm)	w/c	G_F (N/m)	G_f (N/m)
Bazant ZP, Pfeiffer PA	6	29.1–48.4	4.83–12.7	0.5–0.6	–	20.7–40.8
Carpinteri A	2	12.6–16.3	9.52–19.1	0.5–0.6	–	36.3–49
Chang T-P, Shieh M-M	2	30.1–33.9	12.7	0.3	–	34.4–37.2
El-Sayed KM, Guinea GV, Rocco C, Planas J, Elices M	10	43.5–53.5	10–20	0.48	74–141	–
Gettu R, Bazant ZP, Karr ME	2	32.5–85	9.5–13	0.35–0.6	–	21.4–24
Hassanzadeh M	24	82–135	16	0.3–0.4	129–201	–
Hilsdorf HK, Brameshuber W	5	31–35	2–32	0.54	37.6–170	–
Jenq YS, Shah SP	4	25.2–54.8	4.76–19.1	0.25–0.65	–	21.1–30.1
John R, Shah SP	1	110	8	0.22	–	80.16
Karihaloo BL, Nallathambi P	5	26.8–78.2	20	0.2–0.77	–	40–87.8
Malvar LJ, Warren GE	32	29–58.9	10	0.4–0.6	43.6–92.2	–
Mindess S	3	48.5	13	0.38	80.6–115	–
Nallathambi P	36	23.8–44.3	2–20	0.5–0.65	47.2–111	23.4–43
Petersson P-E	14	19.8–85.9	8–16	0.3–0.7	38.8–123	–
Shah SP, Ouyang C, Marikunte S, Yang W, Becq-Giraudon E	10	34.5–87.2	4.76–12	0.29–0.4	–	20.6–62.3
Sok C, Baron J	1	41.3	4.76	0.48	–	62.4
Strange PC, Bryant AH	3	71.1–73.3	2.36–3	0.33–0.53	–	12.2–19.2
Tang T, Ouyang C, Shah SP	3	34.5	3–9.5	0.5	–	25.4–28
Yu BJ, Ansari F	53	3.01–44.6	9.5	0.5	29.8–103	–
Bharatkumar BH, Raghuprasad BK, Ramachandramurthy DS, Narayanan R, Gopalakrishnan S	8	44.69–69.73	12.5	0.36–0.4	93–127	40.4–46.3
Ghaemmaghami A, Ghaemian M	5	31.9–42.7	20–65	0.28–0.53	–	72–178
Tang WC, Lo TY	4	56–89	10–20	0.29–0.48	120–180	–
Einsfeld RA, Velasco MSL	2	48–49	9.5	0.3–0.34	116–129	–
Rao GA, Prasad BKR	8	40–75	4.75–20	0.325	76.6–165	–
Ince R	3	35.3–41.6	4–32	0.6	–	27.3–82.8

Table 3
The range of experimental datasets.

Parameters		Unit	Min	Max	Standard deviation
Inputs	f_c	(MPa)	3.01	135	26.30
	d_{max}	(mm)	2	65	6.68
	w/c		0.2	0.77	0.10
Outputs	G_F	(N/m)	29.8	201	36.60
	G_f	(N/m)	12.2	178	22.81

Table 4
Coding of the different Kriging models.

No.	Base Kriging	Kriging -U learning function	Kriging – K Means clustering		
1	–	U-base	–	–	–
2	Rand-10	U-10	K2-10	K4-10	K6-10
3	Rand-30	U-30	K2-30	K4-30	K6-30
4	Rand-50	U-50	K2-50	K4-50	K6-50

design. Note that in this method the regression and variance coefficients are obtained from Eqs (4) and (5):

$$\beta = \left(1^{\mathrm{T}}\boldsymbol{R}^{\mathrm{T}}1\right)^{-1}1^{\mathrm{T}}\boldsymbol{R}^{\mathrm{T}}\boldsymbol{y} \tag{4}$$

$$\sigma^2 = \frac{(\mathbf{y}-1\beta)^{\mathrm{T}}\mathrm{R}^{-1}(\mathbf{y}-1\beta)}{\mathrm{k}} \tag{5}$$

The correlation between design point pairs is shown by $\mathbf{R}_{ij} = R(\boldsymbol{x}^{(i)}.\boldsymbol{x}^{(j)})$. θ can be calculated using maximum likelihood assessment according to Eq. (6):

$$\theta = arg\ \ min_{\theta}(|\boldsymbol{R}|)^{\frac{1}{k}}\sigma^2 \tag{6}$$

The required predicted response is calculated using Eq. (7).

$$G(x)_{pre} = \beta + \mathrm{r(x)}\boldsymbol{R}^{-1}(\boldsymbol{y}-1\beta) \tag{7}$$

In which r(x) presents the correlation between design points and $\boldsymbol{x}$ (Eq. (8)).

Table 5
Statistical parameters for prediction of fracture energy of concrete.

No.	Name	Abbreviation	Equation
1	Mean squared error	MSE	$MSE = \frac{\sum_1^N (R_{Pre}-R_{Exp})^2}{N}$
2	Root-mean-square error	RMSE	$RMSE = \sqrt{MSE}$
3	Mean absolute error	MAE	$MAE = \frac{\sum_1^N \lvert R_{Pre}-R_{Exp}\rvert}{N}$
4	Sum of squared errors	SSE	$SSE = \sum_1^N \left(\frac{R_{Pre}}{R_{Exp}} - \frac{\overline{R}_{Pre}}{\overline{R}_{Exp}}\right)^2$
5	Correlation Coefficient	R^2	$R^2 = \frac{[\sum_1^N (R_{Pre}-\overline{R}_{Pre})(R_{Exp}-\overline{R}_{Exp})]^2}{\sum_1^N (R_{Pre}-\overline{R}_{Pre})^2 \sum_1^N (R_{Exp}-\overline{R}_{Exp})^2}$
6	Standard deviation	SD	$SD = \sqrt{\frac{\sum_1^N \left(\frac{R_{Pre}}{R_{Exp}} - \frac{\overline{R}_{Pre}}{\overline{R}_{Exp}}\right)^2}{N-1}}$

$$r(x) = \left\{R\left(\theta.\boldsymbol{x}.\boldsymbol{x}^{(1)}\right).R\left(\theta.\boldsymbol{x}.\boldsymbol{x}^{(2)}\right).....R\left(\theta.\boldsymbol{x}.\boldsymbol{x}^{(n)}\right)\right\} \tag{8}$$

The value of the kriging model variance for the predicted values, σ^2_{pre}, can be driven by calculating the minimum mean square errors between the existing response, $G(x)$ and the corresponding prediction response, $G(x)_{pre}$, according to Eq. (9).

$$\sigma^2{}_{pre} = \sigma^2\left[1 + \mathrm{u}(\boldsymbol{x})^T\left(1^{\mathrm{T}}\boldsymbol{R}^{\mathrm{T}}1\right)^{-1}u(\boldsymbol{x}) - r(\boldsymbol{x})^T\boldsymbol{R}^{-1}r(\boldsymbol{x})\right] \tag{9}$$

where $u(\boldsymbol{x}) = 1^{\mathrm{T}}\boldsymbol{R}^{-1}\boldsymbol{r}(\boldsymbol{x}) - 1$.

An optimal number of design points must be used to achieve accurate prediction (the actual performance function) using the Kriging method. Because, if a small number of design points is used, the accuracy of Kriging method will not be acceptable and if a lot of learning points are used, the efficiency of this method will be reduced [67,68]. In the basic Kriging method, if the number of design points set is large, the learning

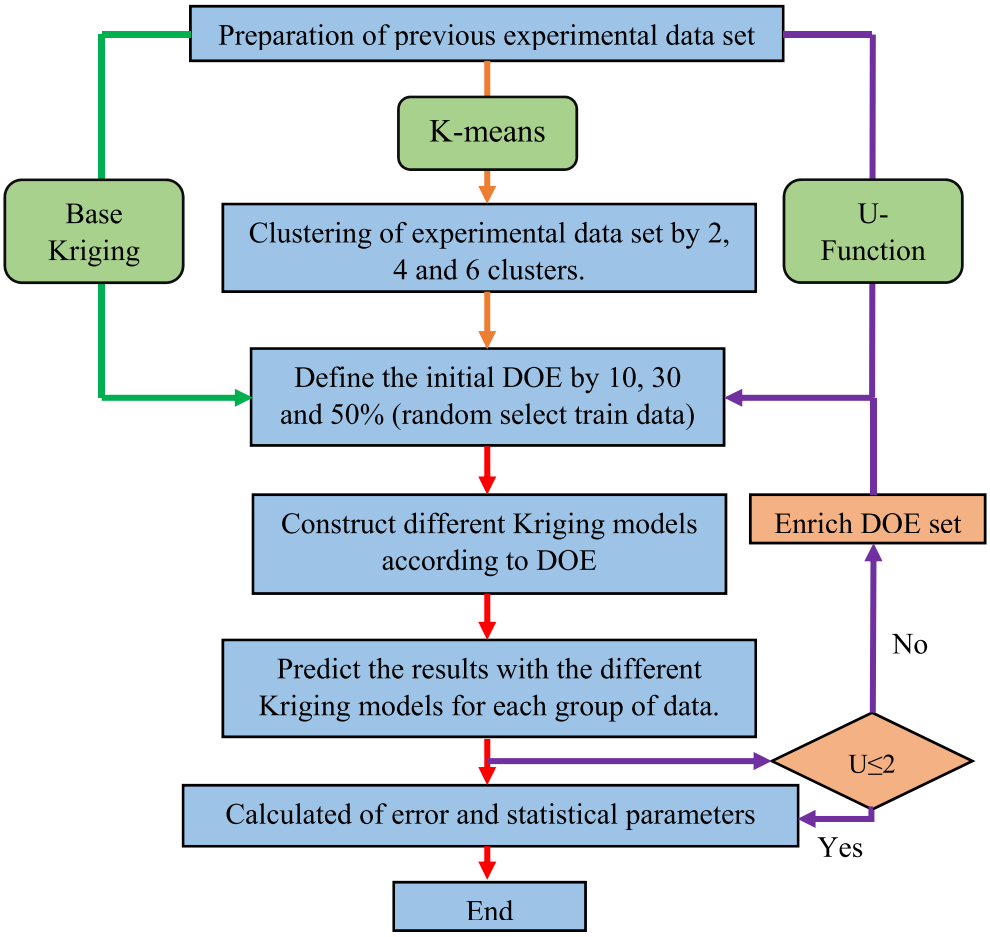

Fig. 2. Flowchart of the proposed different kriging models.

data are usually selected randomly from the data set. However, achieving the desired accuracy in these models requires increasing the number of members of the sample points set (based on DoE), which are often added randomly or unconsciously to this set. Adding new sample points to the set of design points unconsciously, will not always lead to more accurate results. This is because the cost and time of computing may increase when more members are in the design points set.

5. U learning function

In the past, the proposed Kriging models were presented inactive or fixed with the introduction of many points based on DoE concepts [69]. But Kriging's ability to determine the variance of the estimated data makes it possible to improve the DoE points with the help of an adaptive structure. To increase the accuracy of result prediction, when there is data with high variance, that point will be added to the DoE data set [48]. It is difficult to achieve the desired level of accuracy and computational costs at the same time in the basic Kriging model. This is because the basic Kriging model does not have the ability to detect a sufficient number of DoE points (selected by the user) to complete learning and have an accurate prediction. The concept of active learning is proposed to solve this problem. Using this concept, the data with the ability to increase the accuracy and quality of Kriging results are added to the system in each stage as new training data so that they can cover more limitations and provide the desired level of accuracy and computational cost [70,71]. This modeling method is called active learning Kriging (ALK).

The U-learning function is based on the concept of the distance between the estimated values and the actual values, as well as the standard deviation of the estimated values. The potential of the desired point that must be added in order to correct and improve the DoE points set is determined using this learning function [71].

This learning function is defined by Eq. (10):

$$U(x) = \frac{|R_{Pre}|}{\sigma_{R_{Pre}}} \tag{10}$$

where R_{Pre} and $\sigma_{R_{Pre}}$ are the predicted value and standard deviation of the Kriging model. Any point that has a lower $U(x)$ value will be defined as a new point that must be added to the DoE points set. The small value of the $U(x)$learning function indicates that either the predictive value is too small $(R_{Pre} \rightarrow 0)$ or $\sigma_{R_{Pre}}$ has a high value. In some cases these two states occurred simultaneously [67]. There is a high risk potential and uncertainty for the point with the Kriging model prediction value of zero. This point is selected as the new point based on Eq. (11).

$$x_{add} = argmin[U(x)] \tag{11}$$

The $min[U(x)] \geq 2$ condition must be met to achieve the correct precision of the active Kriging model. Because when $U(x) = 2$ with the probability of $\Phi(2) = 0.977$, there will be a true judgment of the desired point [72].

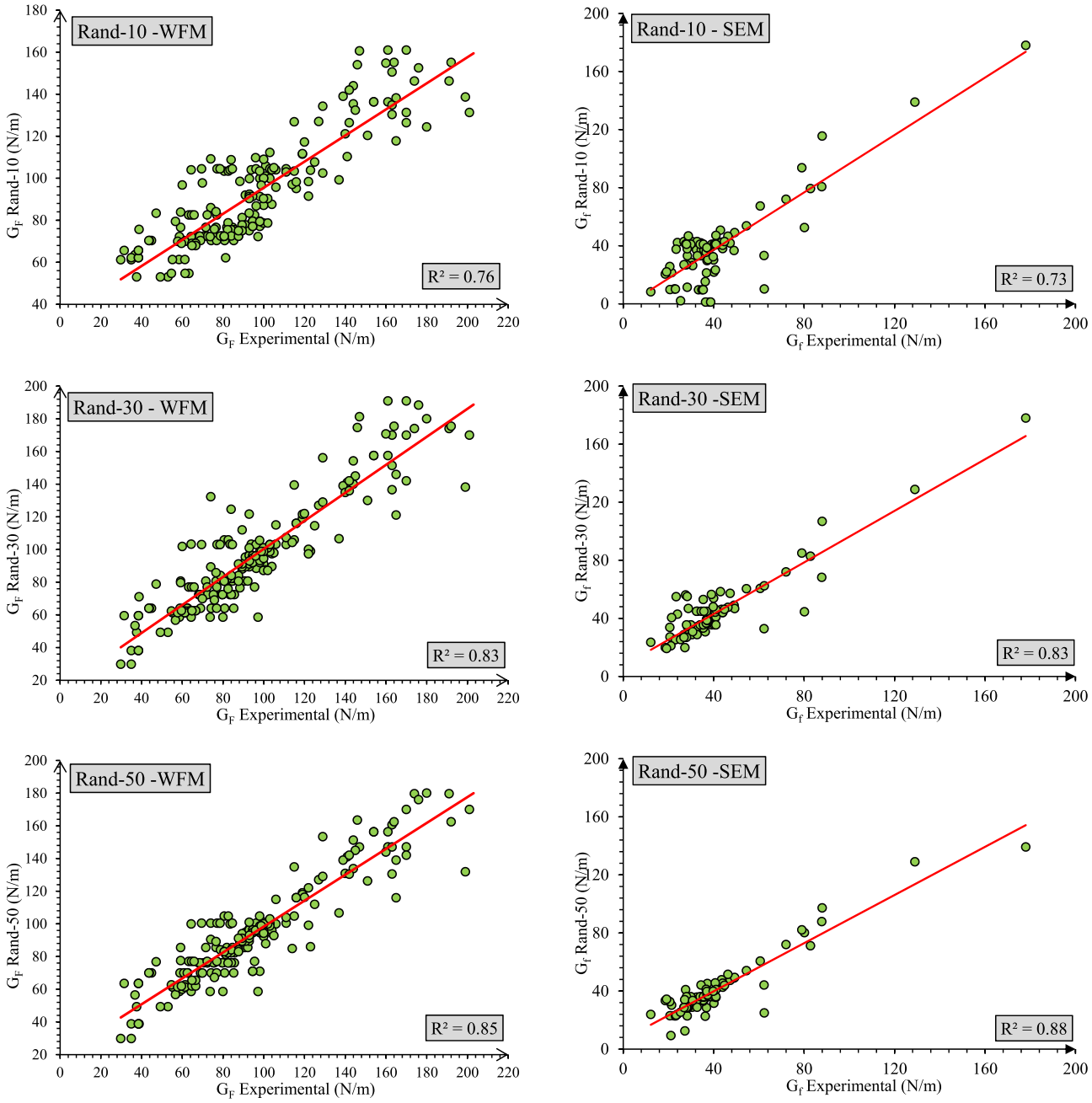

Fig. 3. Results of base kriging models and experimental G_f and G_F.

6. K-means clustering

The unsupervised classification process (clustering) is used to classify and place the data with similar characteristics in the same groups [73, 74]. K-means clustering is widely used for data sets classification in K cluster. Despite the simplicity and power of discovering the hidden patterns of the data set, as well as the very good convergence rate of K-means clustering in achieving the optimal local point, the use of this method is limited. These limitations are due to introducing the number of clusters (K) before the clustering starts and the random selection of cluster centers [74,75]. The steps of data classification using the K-means method are as follows:

1 The user selects the number of clusters.
2. K points which are actually the centers of the clusters are selected randomly.
3. By comparing the distance of the available data with each of the cluster centers, the data are placed in the closest cluster.
4. The cluster centers are updated according to the mean of the cluster centers.
5. Based on the new center, the data will be classified again. In this case, one point may be placed in another new cluster.
6 Steps 3, 4, and 5 will be repeated until the centers are fixed and the clusters converge.

7. Test data and input and output parameters

A data set collected by Nikbin et al. [23] where used in this study to

Table 6
Results of statistical parameters of different models and equations for G_F.

Statistical parameters	Rand-10	Rand-30	Rand-50	U-base	U-10	U-30	U-50	K2-10	K2-30	K2-50	K4-10	K4-30	K4-50	K6-10	K6-30	K6-50	Bazant and Becq-Giraudon [56]	CEB-90 [57]	CEB-2010 [58]	JSCE [59]	JSCE
	163.8	127.1	103.1	180.4	150.1	121.3	98.5	204.6	178.2	125.1	160.3	141.1	131.1	173.3	152.2	134.9	331.8	980.4	232.4	1867.3	427.2
RMSE	12.8	11.3	10.2	13.4	12.3	11.0	9.9	14.3	13.3	11.2	12.7	11.9	11.5	13.2	12.3	11.6	18.2	31.3	15.2	43.2	20.7
MAE	14.5	10.1	9.1	15.3	12.8	9.2	7.9	18.2	11.9	10.7	16.9	16.4	9.8	14.9	12.4	11.4	18.8	29.1	20.7	55.3	22.4
R^2	0.76	0.83	0.85	0.66	0.77	0.85	0.88	0.59	0.79	0.83	0.66	0.71	0.84	0.68	0.80	0.80	0.66	0.66	0.69	0.61	0.66
SSE	14.7	8.1	7.2	14.7	10.0	7.1	4.3	14.5	7.2	6.7	14.5	18.9	4.8	16.4	9.9	9.0	14.2	29.5	15.1	88.2	12.1
SD	0.3	0.2	0.2	0.3	0.2	0.2	0.1	0.3	0.2	0.2	0.3	0.3	0.2	0.3	0.2	0.2	0.3	0.4	0.3	0.7	0.2

predict the fracture energy of the concrete as an output parameter. A total of 246 data series where used. In order to summarize the information, the values of the input and output parameters are shown as domains in Table 2. Table 3 shows the details of each parameter. Many researchers have investigated the effects of various parameters such as aggregate type, aggregate content, aggregate size distribution, curing temperature and conditions, loading rate, high temperature (fire) and fracture path on the fracture energy [30,76–81]. But, the input parameters are selected in such a way that the general characteristics of concrete are expressed with a good adaptation to the parameters used in Table 1 equations, in addition to the tangible effect on the fracture energy value and availability. Compressive strength, maximum aggregate size and water to cement ratio are considered as input parameters in this study.

8. Methodology

In prediction methods such as neural networks and ANFIS, determining a certain percentage of data for better network learning and providing an accurate model for estimating the engineering properties and materials is a big problem and in most cases, a lot of basic data sets are needed. In this study, the Kriging method, U-learning function and K-means clustering where combined to assess models that show the best performance in concrete fracture energy estimation with the lowest percentage of learning data. Due to the basic Kriging state, the use of active learning function and clustering (A) and the percentages of 10, 30, and 50 (B) to select the learning data, the proposed models are named as code (A-B). The coding of the different models is shown in Table 4. In this study, the *U* index is considered to be 2 for the active learning function. In the case of combining the Kriging and K-means clustering methods, three cases of 2, 4 and 6 clusters were investigated to provide a stronger model. To investigate the accuracy and efficiency of the proposed Kriging models, the mean squared errors (MSE), the root mean squared error (RMSE), the mean absolute error (MAE), sum of squared errors (SSE), the correlation coefficient (R^2) and the standard deviation (SD) were used. More detailed information on these parameters and their relationships are given in Table 5. Fig. 2. Shows flowchart of prediction of concrete fracture energy.

9. Results and discussion

9.1. Base kriging models

Fig. 3 shows the G_f and G_F results of the base Kriging models versus experimental results. The results of the statistical parameters are given in Table 6 and Table 7 to examine the accuracy of the basic Kriging models. According to Tables 6 and 7, considering the aggregate shape, the WFM and SEM fracture energy prediction for all basic Kriging models have less error compared to the previous available relationships. However, predicting the fracture energy in the WFM using the basic Kriging models has a better accuracy than the SEM. The use of 10%, 30%, and 50% of the data as DoE points in WFM results in 72%, 88%, and 98% reductions in the MSE parameter relative to the Bazant and Becq-Giraudon [56] relationship. In the WFM, the MSE parameter of the Kriging model designed with 50% of the data compared to CEB-90 [57], CEB-2010 [58] and JSCE [59] relationships decreased by 55.6%, 94.5% and 75.9%, respectively. When the number of learning data is 10%, 30%, and 50%, the MSE value of the SEM will have 59.1%, 80%, and 87.2% decrease, respectively (relative to the Bazant and Becq-Giraudon [56] relationship). The SSE values of the energy prediction results of the SEM are in the range of 4.92 ro 14.22. But considering the round and broken shape of the aggregates, the value of SSE in the Bazant and Becq-Giraudon [56] for G_f estimation is 14.77 and 30.62, respectively. The SSE parameter of the G_F prediction results for the Bazant and Becq-Giraudon [56], CEB-90 [57], CEB-2010 [58], and JSCE [59] relationships are equal to 14.24, 15.07, 88.23, and 12.40, respectively.

Table 7
Results of statistical parameters of different models and equations for G_f.

Statistical parameters	kriging models													Bazant and Becq-Giraudon [56]	
	Rand-10	Rand-30	Rand-50	U-base	U-10	U-30	U-50	K2-10	K2-30	K2-50	K4-10	K4-30	K4-50	Round aggregates	Crush aggregates
MSE	204.1	99.7	63.6	145.9	112.3	59.3	44.9	159.6	126.2	34.1	124.4	94.9	24.3	497.8	500.2
RMSE	14.3	10.0	8.0	12.1	10.6	7.7	6.7	12.6	11.2	5.8	11.2	9.7	4.9	22.3	22.4
MAE	9.6	5.8	4.3	8.7	7.5	4.9	3.7	8.5	5.9	2.8	7.9	5.5	2.8	11.4	15.4
R^2	0.73	0.83	0.88	0.82	0.82	0.90	0.92	0.71	0.81	0.93	0.80	0.83	0.95	0.14	0.14
SSE	14.2	8.1	4.9	10.7	6.5	4.1	3.8	8.4	4.9	2.6	8.7	4.8	2.8	14.8	30.6
SD	0.4	0.3	0.2	0.3	0.3	0.2	0.2	0.3	0.2	0.2	0.3	0.2	0.2	0.4	0.6

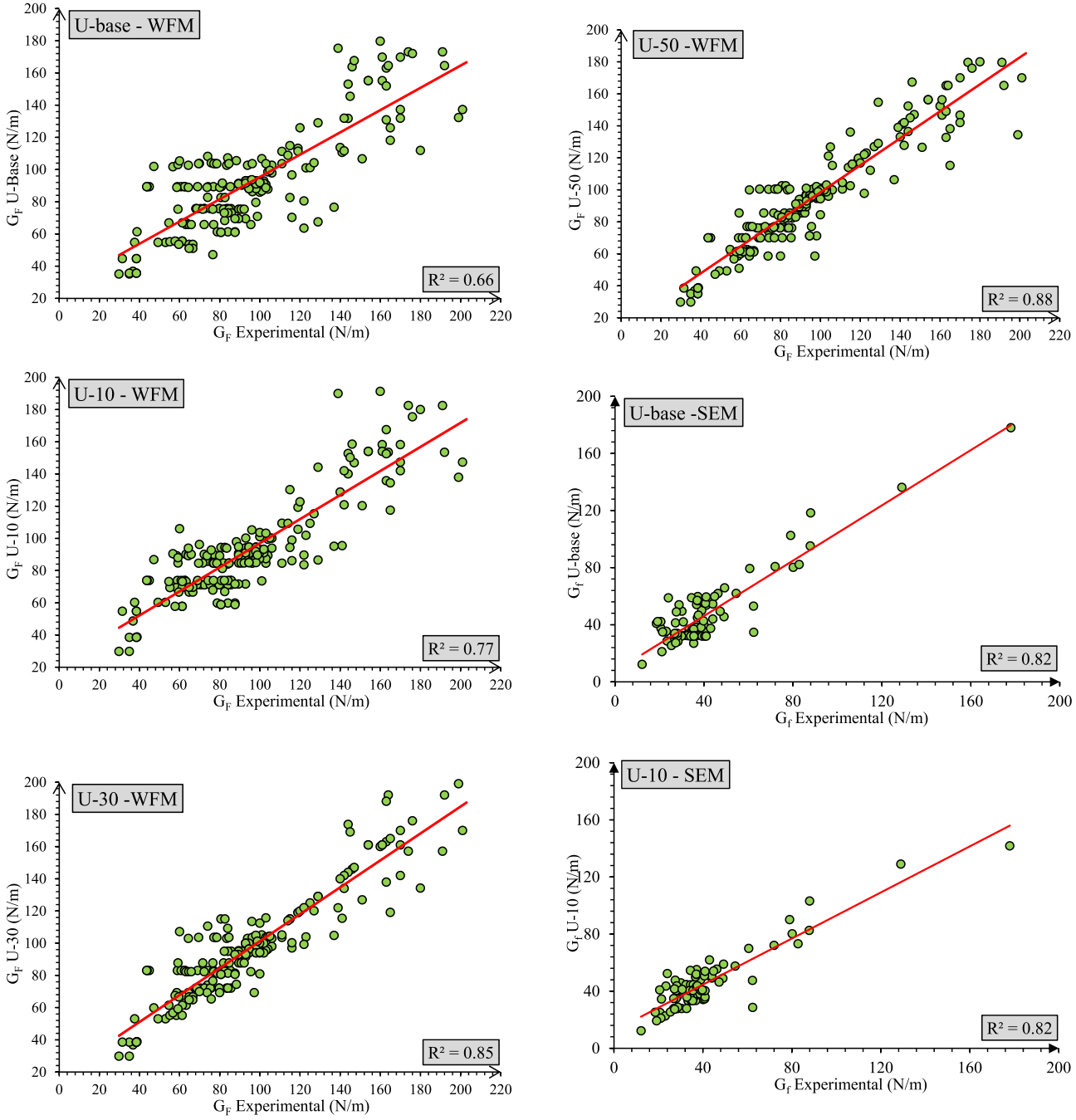

Fig. 4. Results of kriging- U-function models and experimental G_f and G_F.

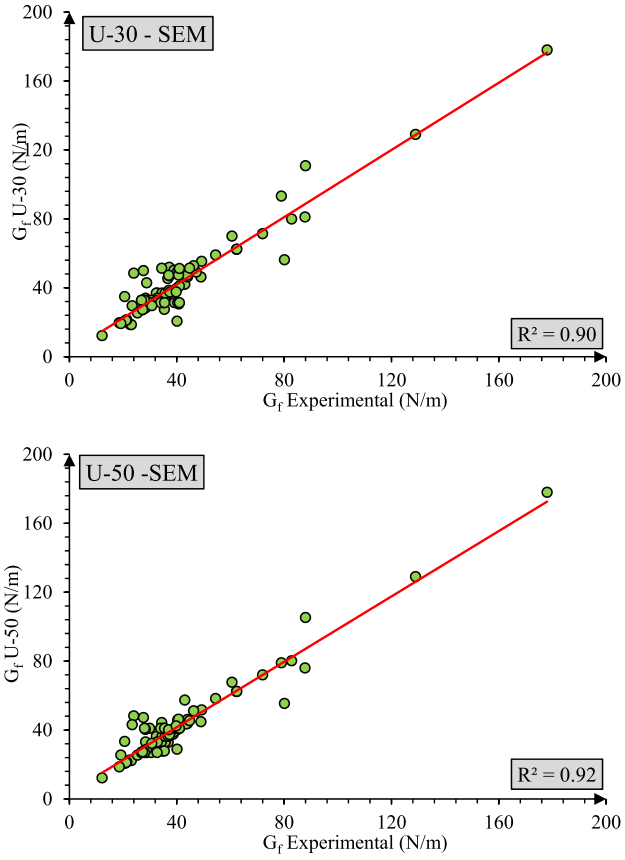

Fig. 4. (*continued*).

Selecting 10% of the data as the DoE points in the basic Kriging model makes the size effect and work fracture methods to have an SD value almost equal to that of Bazant and Becq-Giraudon [56] relationship. However, compared to the Bazant and Becq-Giraudon [56], the use of 30% and 50% of the available data for learning basic kriging models in SEM has reduced the SD parameter by 26.07% and 42.28%, respectively. The SD parameter of the Rand-50 model in WFM reduced by 29.02%, 30.99%, 71.48%, and 23.12% relative to the Bazant and Becq-Giraudon [56], CEB-90 [57], CEB-2010 [58], and JSCE [59] relationships, respectively. According to Fig. 3, the value of the correlation coefficient (R^2) for the Rand-10, Rand-30, and Rand-50 models in the size effect and fracture work method is 0.76, 0.83, 0.85, 0.73, 0.83 and 0.88, respectively. While for the Bazant and Becq-Giraudon [56] relationship, the R^2 values in WFM and SEM methods with different shape aggregates are 0.14 and 0.66, respectively. This indicates that the shape of the aggregates does not affect the value of the correlation coefficient in the Bazant and Becq-Giraudon [56] relationship. On the other hand, the correlation coefficients of CEB-90 [57], CEB-2010 [58], and JSCE [59] in the WFM are less than 0.70. These results indicate a mismatch between the results of these relationships and the available experimental data. In WFM and SEM, the introduction of 50% of the collected data as the DoE points of the base Kriging model has significantly increased the correlation coefficient value ($0.85 \leq R^2$).

According to Table 7 the average error values of the Rand-10, Rand-30 and Rand-50 models for G_f prediction are to 27.7%, 16.4% and 12.2%, respectively. Using 10%, 30% and 50% of the data in the WFM in order to create the basic Kriging model, causes the average error values to be 18.2%, 12.2% and 10.6%, respectively. This means that the performance of the basic Kriging models in the WFM fracture energy prediction process is much better than that of SEM. The average error value of the Bazant and Becq-Giraudon [56] in the SEM is 20.7%, which only performs better than Rand-10. The Bazant and Becq-Giraudon [56], CEB-90 [57], CEB-2010 [58], and JSCE [59] relationships in the WFM are 21%, 24.4%, 78.6%, and 22.5% of the average error, respectively. These relationships have a higher average error than the basic Kriging models created using 10%, 30%, and 50% data for learning. Comparing the average values of the base Kriging and the neural networks models provided by Nikbin et al. [23] (19.8%), which were obtained using 70% of the data for network training, it is determined that using 30% and 50% of the data to learn the basic Kriging model in the SEM will result in a lower average error value. However, even introducing 10% of the data as DoE in WFM, results in 8.8% reduction of the average error value compared to the neural network model provided by Nikbin et al. [23].

9.2. *Combining Kriging models with U-function*

The fracture energy predicted by combined Kriging models and the U-learning function versus available experimental data is in Fig. 4. According to Tables 6 and 7, the MSE values of the U-Base, U-10, U-30, and U-50 models in the SEM had 70.7%, 77.4%, 88.1%, and 91% reduction, respectively, compared to the Bazant and Becq-Giraudon [56]. The MSE improvement of these models in the WFM compared to the Bazant and Becq-Giraudon [56] relationship is in the range of 45–70. The MSE values of the U-50 compared to the CEB-90 [57], CEB-2010 [58], and JSCE [59] in WFM are improved by 57.6%, 94.7% and 77%, respectively. Increasing the number of training data from 10% to 50% has improved the MSE in WFM and SEM by 60% and 34.4%, respectively. The reduction of SSE parameter in U-10, U-30 and U-50 models in WFM and SEM compared to the Bazant and Becq-Giraudon [56] relationship are in the range of 29%–70% and 55%–75%, respectively. All combined Kriging Models and U-learning functions have a lower SSE than CEB-90 [57], CEB-2010 [58], and JSCE [59]. For the previous available

Table 8
Error of different models and equations.

Method	Error	kriging models												Code equations				
		Rand-10	Rand-30	Rand-50	U-base	U-10	U-30	U-50	K2-10	K2-30	K2-50	K4-10	K4-30	K4-50	K6-10	K6-30	K6-50	Bazant and Becq-Giraudon [5]	CEB-90 [42]	CEB-2010 [30]	JSCE [31]
Size effect method (SEM)	Min	0.47	0.51	0.56	0.41	0.46	0.50	0.50	0.52	0.57	0.50	0.54	0.50	0.53	–	–	–	0.34	–	–	–
	Max	3.66	1.90	1.60	1.31	1.31	1.42	1.39	3.20	1.60	1.38	2.26	2.16	1.53	–	–	–	3.53	–	–	–
	Average (%)	27.7	16.4	12.2	21.8	19.6	12.1	9.8	22.0	14.0	7.1	21.6	12.9	6.2	–	–	–	20.74	–	–	–
Work of-fracture method (WFM)	Min	0.48	0.53	0.54	0.46	0.54	0.56	0.62	0.43	0.56	0.64	0.47	0.47	0.58	0.37	0.52	0.58	0.45	0.49	0.25	0.53
	Max	1.53	1.44	1.43	1.92	1.49	1.40	1.38	2.72	1.80	1.56	1.93	1.89	1.71	2.06	1.75	1.45	2.20	3.18	1.21	1.94
	Average (%)	18.1	12.2	10.6	17.9	15.3	10.8	8.8	19.5	13.4	12.3	19.2	18.3	10.5	18.5	15.2	12.7	21.0	24.4	78.6	22.5

relationships and combined Kriging models, SSE parameter is between 12.1-88.2 and 4.3–14.7, respectively. The SD value of combined kriging models and previous relationships in WFM are in the ranges of 0.15–0.27 and 0.25–0.67, respectively. The worst performance (SD = 0.67) among previous existing relationships belongs to JSCE [59]. Compared to the Bazant and Becq-Giraudon [56] relationship, the increase of training data from 10% to 50% in the Kriging combination models used in the SEM has improved SD parameter by 33.6%, 47.1% and 49.1%, respectively.

According to Fig. 4, the increase in training data in combined Kriging models with the U- function in both WFM and SEM has reduced the dispersion of the prediction data. Fig. 4 shows that the reduction in data dispersion is more evident in the SEM than the WFM. In the WFM, the correlation coefficient of all existing relationships is between 0.61 and 0.69. In WFM, only the R^2 value of the U-Base model is in this range. However, the values of this parameter for the U-10, U-30 and U-50 models are 0.77, 0.85, and 0.88, respectively. The R^2 values of the U-Base, U-10, U-30, and U-50 models in SEM are 0.82, 0.82, 0.90, and 0.92, respectively. Considering the shape of aggregates, this parameter will have a value of 0.14 for the Bazant and Becq-Giraudon [56] relationship, which indicates the high dispersion of the data predicted by this relationship.

The mean error of the U-base, U-10, U-30, and U-50 models in SEM is 21.8%, 19.6%, 12.1% and 9.8%, respectively (Table 8). Compared to the mean error of the Bazant and Becq-Giraudon [56] relationship (20.7%), the use of 10%, 30%, and 50% of the data as DoE points, causes 5.7%, 41.9%, and 53% decreases, respectively in SEM. But the U-base model has a 5.3% increase in the mean error compared to the Bazant and Becq-Giraudon [56] relationship. Generally, the mean error of the U-10, U-30, and U-50 models in SEM compared to the Nikbin et al. [23] neural network model (19.8%) has improved 1.2%, 39.1%, and 50.8%, respectively. In the WFM, the U-base, U-10, U-30 and U-50 models have mean errors of 17.9%, 15.3%, 10.8%, and 8.8%, respectively. The Bazant and Becq-Giraudon [56], CEB-90 [57], CEB-2010 [58] and JSCE [59] relationships have mean errors of 21%, 24.4%, 78.6 and 22.5%, respectively, in WFM. The mean error of the G_F prediction process by the U-50 model, show improvements of 58.1%, 63.8%, 88.8%, and 60.9% relative to the Bazant and Becq-Giraudon [56], CEB-90 [57], CEB-2010 [58], and JSCE [59] relationships, respectively. Although the Nikbin et al. [23] model predicts 19.8% error in the fracture energy of WFM, the U-base, U-10, U-30, and U-50 models improved the prediction error for 9.8%, 22.8%, 45.2%, and 55.6%, respectively.

9.3. *Combining Kriging models with K-Means clustering*

The available experimental data versus the predicted results of the combined Kriging models and K-means clustring are shown in Fig. 5 and Fig. 6. Tables 6 and 7 show the results of the statistical parameters MSE, RMSE, MAE, SSE, and SD of the proposed models and the available relationships. In SEM, the use of more training data and clusters has led to a reduction in the MSE value of the proposed models. In this method, the MSE parameter for K2-10, K2-30, and K2-50 models is in the range of 34.12–159.57. This parameter is in the range of 24.27–124.35 for the K4-10, K4-30, and K4-50 models. Despite the slight difference in the SSE values of the models generated based on K = 2 and K = 4, these clusters have almost the same SD parameters. The MSE values of the fracture energy prediction on WFM by models created based on K-means, for the cases with the number of clusters equal to 2, 4, and 6, are in the ranges of 125.13–204.58, 131.10–160.30, and 134.90–173.29, respectively. The dispersion of this parameter in WFM is more than SEM. According to Tables 6 and 7, the K4-50 model shows the best performance in fracture energy estimation compared to proposed models in WFM and SEM. The use of 6 clusters for data classification while G_F estimation has led to an increase in the statistical parameters compared to the case where K = 4. Data clustering in SEM has no effect on the SD parameter of Kriging and K-means combined models. The SD value of the K2, K4, and K6 models

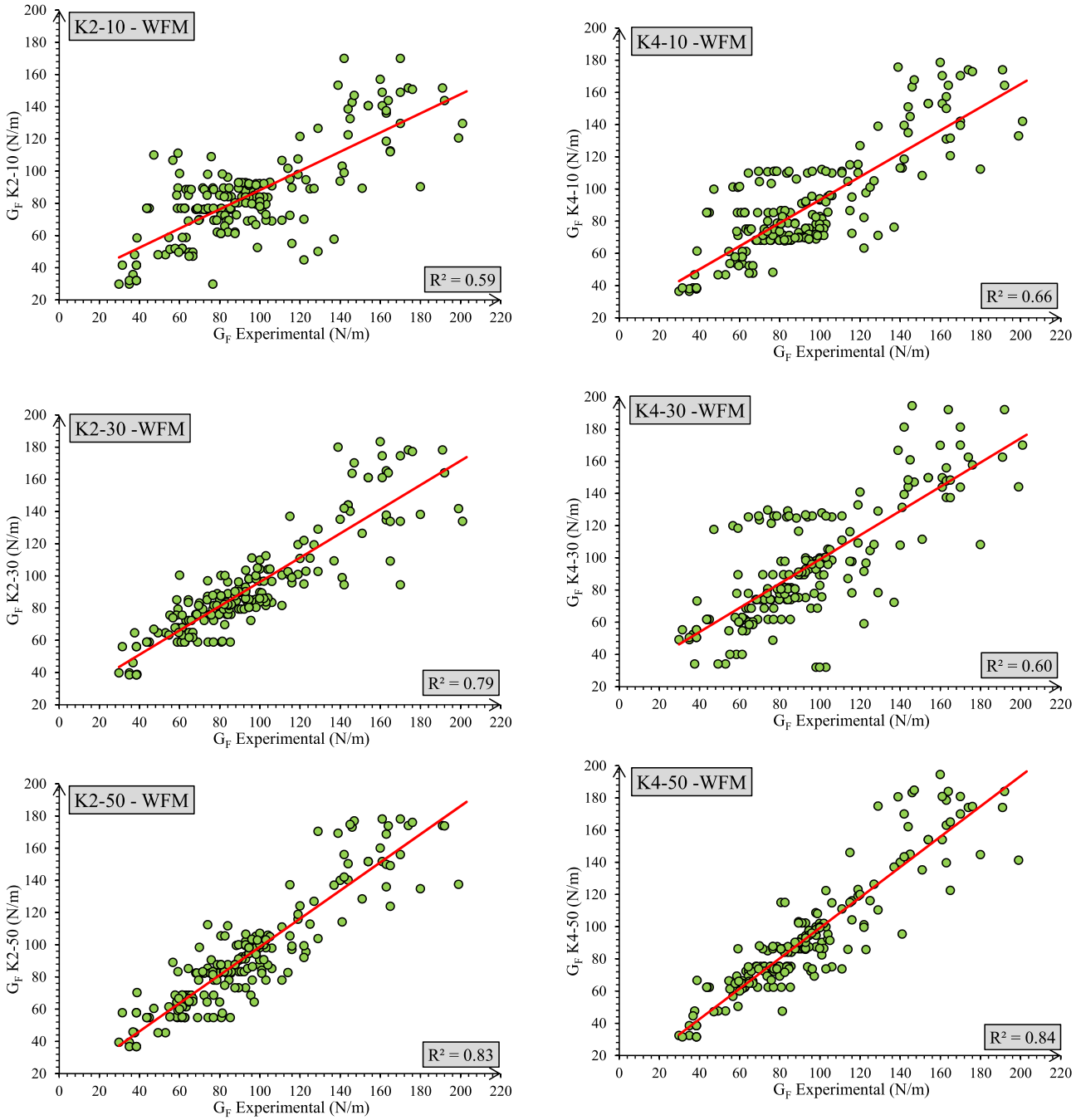

Fig. 5. Results of kriging- K-means models and experimental G_F.

generated by introducing 10%, 30%, and 50% of the data as DoE in WFM, is less than 0.30. However, the value of this parameter for the proposed models is still lower than the SD of Bazant and Becq-Giraudon [56] relationship (0.41). In WFM, the SD values of Bazant and Becq-Giraudon [56], CEB-90 [57], CEB-2010 [58], and JSCE [59] relationships are greater than 0.25. Comparing the results of K2-50 and K4-50 models in SEM with the results obtained the Bazant and Becq-Giraudon [56] relationship; 93.15% and 95.12% improvements in MSE parameters are presented, respectively. While compared to the Bazant and Becq-Giraudon [56] relationship, the improvement of this parameter in WFM, is equal to 62.30%, 43.64%, and 59.35% for K2-50, K4-50, and K6-50 models, respectively. Compared to the K4-50 model, CEB-90 [57], CEB-2010 [58], and JSCE [59] relationships have shown an increase in MSE of about 43.58%, 92.98%, and 69.31%, respectively. Considering the broken shape of aggregates has a negative effect on G_F results prediction in the Bazant and Becq-Giraudon [56] relationship. In WFM, the data classification in 2, 4, and 6 clusters causes the SSE value to be in the ranges of 6.7–14.5, 4.8–13.5, and 9–16.4, respectively. However, the SSE range for the models generated based on 2 and 4 clusters in SEM is 2.6–8.7. The SSE value of the Bazant and

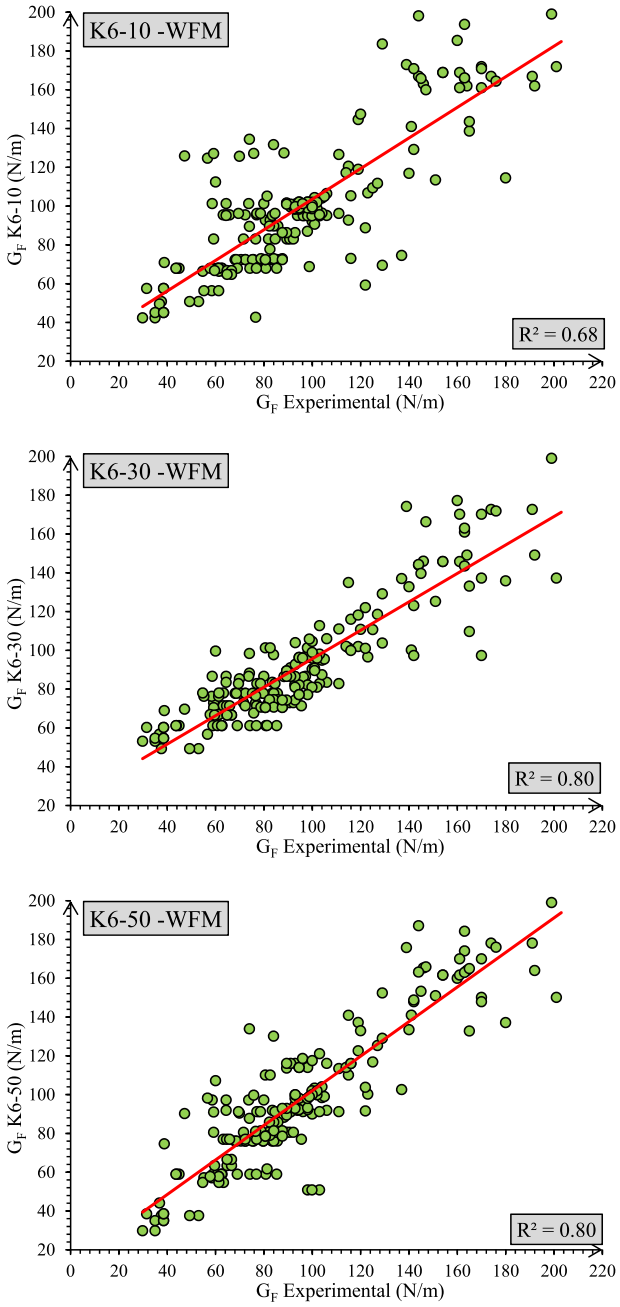

Fig. 5. (*continued*).

Becq-Giraudon [56] relationship in SEM is equal to14.77. CEB-90 [57], CEB-2010 [58], and JSCE [59] relationships have SSE values of 14.24, 15.77, 88.23, and 12.14, respectively.

Compared to the Bazant and Becq-Giraudon [56] relationship, the use of 2 and 4 clusters for data bank classification in SEM, increased the correlation coefficient (R^2) significantly. In WFM, the R^2 value of all the combined kriging and K-means models is in the range of 0.59–0.84 and all previous relationships are in the range of 0.61–0.69. According to Tables 6 and 7, in the case of selecting 50% of the data for learning in WFM, the R^2 value does not change significantly with the increase in number of clusters from 2 to 6. While compared to WFM, the increase in the number of clusters from 2 to 4 in SEM has had a significant effect on the performance of different models. The weakest performance in this method is belongs to different clustering cases and the use of 10% of the data for training.

According to Table 8, the mean error value of the proposed Kriging models for the fracture energy prediction in the WFM is in the range of 10.5%–19.5%. While in WFM, Bazant and Becq-Giraudon [56], CEB-90 [57], CEB-2010 [58] and JSCE [59] relationships have 21%, 24.4%, 78.6% and 22.5% mean error, respectively. There are improvements in mean error values of the combined Kriging and K-means models compared to Nikbin et al. [23] model. The mean error of the weakest (K2-10) and strongest (K4-50) Kriging model compared to the Nikbin et al. [23] model decreased by about 0.3% and 46.75%, respectively. The assessment of the maximum and minimum results in Table 8 shows that the mean error of the fracture energy prediction by Kriging models in SEM is more expanded than that of WFM. However, the results predicted by Kriging and K-means combined models have an acceptable consistence with the experimental results in SEM, compared to WFM. Fig. 7 shows the different clusters in WFM and SEM.

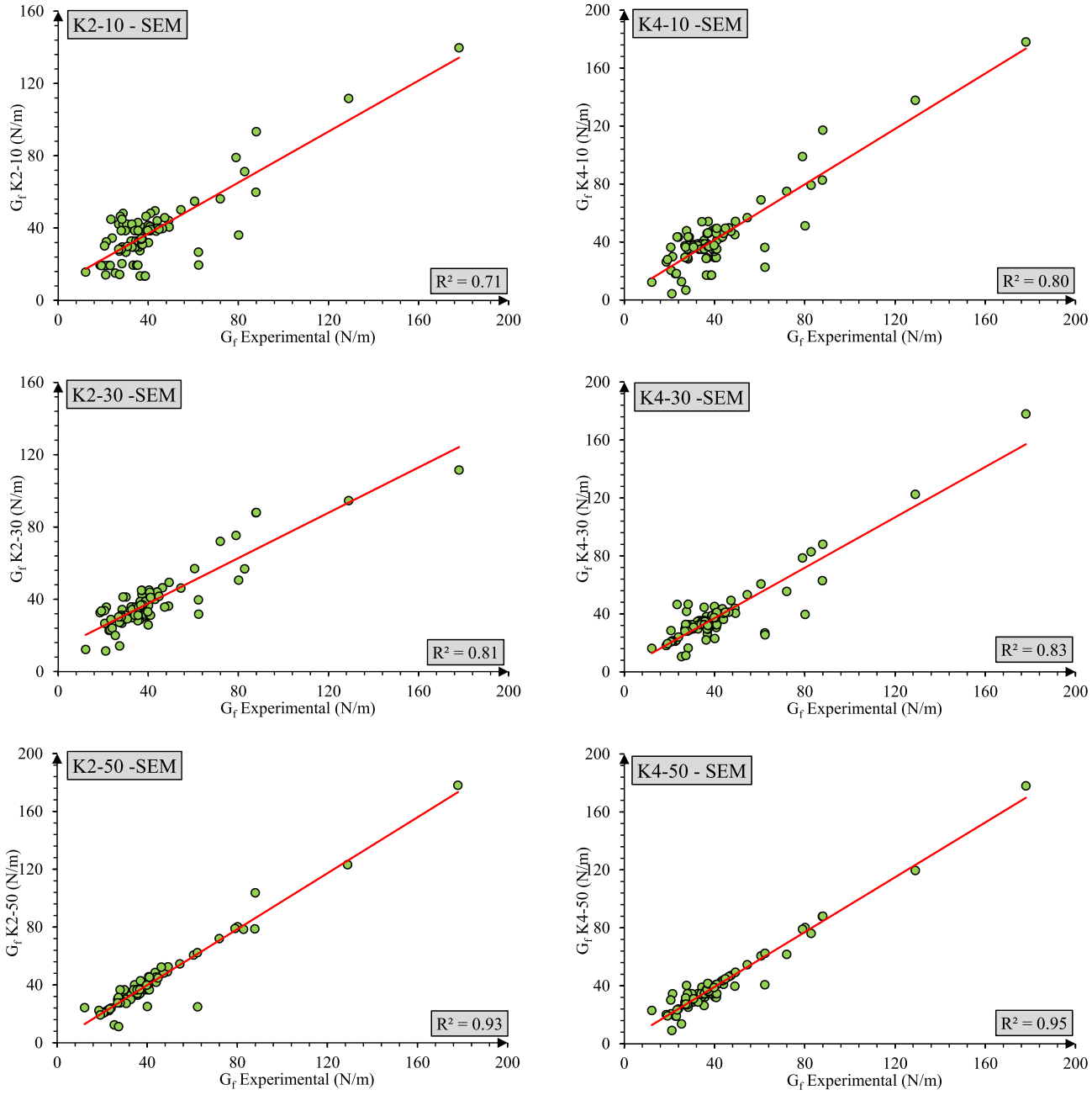

Fig. 6. Results of kriging- K-means models and experimental G_f.

9.4. *The relationship between G_F and G_f*

The fracture energy obtained from SEM is typically less scattered and does not depend on the size and shape of the sample. Calculating fracture energy in this method is more useful than WFM fracture energy and can be calculated more easily. Determining G_F/G_f is very useful in practical applications, especially when element analysis depends on the fracture phenomenon. Due to the high uncertainty in direct determination of G_F value, it is suggested to calculate this parameter indirectly and by means of G_f. The appropriate G_F/G_f value for typical concrete is reported to be in the range of 2–2.5 [60]. However, according to Bazant and Becq-Giraudon [56], the value of G_F/G_f is equal to 2.5. According to Table 9, the G_F/G_f values for Rand-10, Rand-50, K2-30, and K4-30 are greater than 2.5, but this ratio is in the range of 2–2.5 for the rest of the models. The lowest and highest G_F/G_f values are U-base and Rand-10, respectively. The results indicate that for the lower percentages of training data selection, the G_F/G_f ratio tends to the lower limit (2) and for the higher percentages this ratio will tend to the higher limit (2.5). As can be seen in Table 9, when $K = 2$ the G_F/G_f results are close to each other. The most dispersed G_F/G_f results belong to Rand-10 model.

10. Conclusions

In this study, a database of 246 data sets was collected from past studies in which compressive strength, water-to-cement ratio and maximum aggregate size are considered as input parameters and the

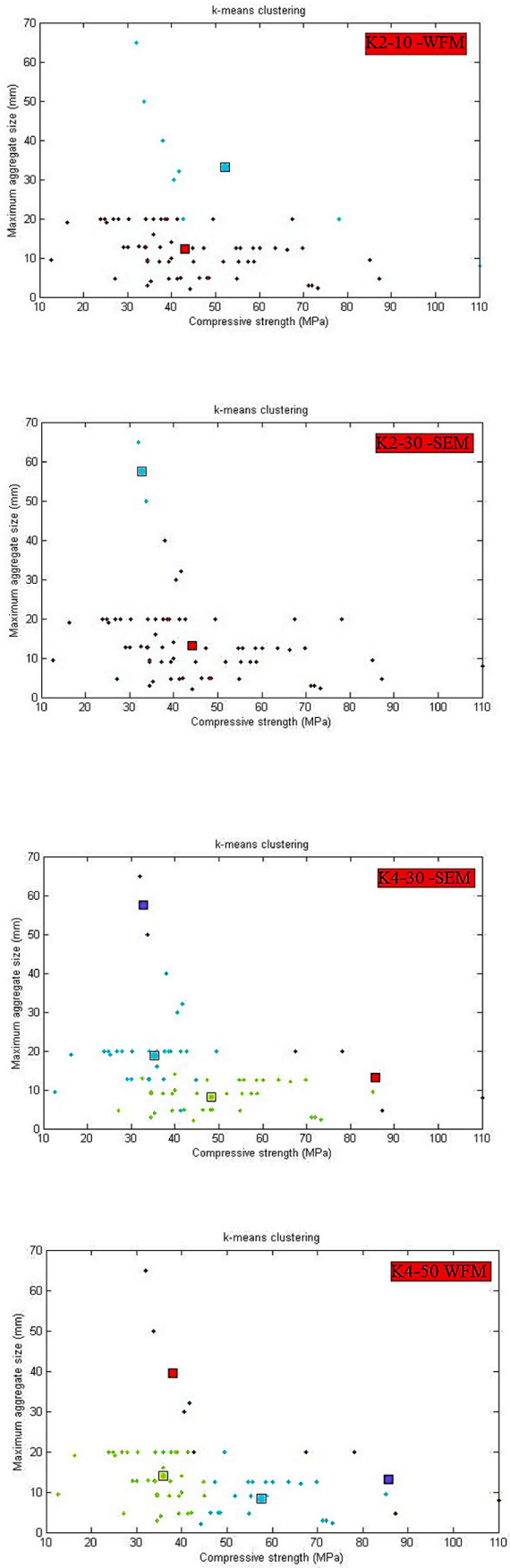

Fig. 7. Different clusters in WFM and SEM.

fracture energy as the output. In order to predict the fracture energy parameter of concrete, Kriging surrogate method was used by selecting 10%, 30%, and 50% of the data for training and combining this method with U-learning function and K-Means clustering. After analyzing the performance of the proposed Kriging models and comparing them with previously available relationships, the following results were obtained:

- The use of basic Kriging models in WFM is more efficient for fracture energy prediction compared to SEM. The statistical parameters (MSE, RMSE, MAE, SSE, and SD) of all basic Kriging models decreased compared to the Bazant and Becq-Giraudon [56], CEB-90 [57], CEB-2010 [58], and JSCE [59] relationships.
- In SEM, the use of the U- learning function has improved the prediction results of the proposed combined models compared to the basic kriging models and previously available relationships. Combining Kriging models with K-means and using 50% of the database compared to the basic Kriging models, using the U-function and previous existing relationships will lead to more accurate prediction results.
- The use of K-means in WFM to predict the fracture energy compared to basic Kriging models and the U-function has reduced the accuracy of the results. However, with the exception of the K2-10 model, the combination of the Kriging and K-means has provided better results than ones presented by the previous efforts. Increasing the number of clusters from 2 to 6 in WFM has reduced the result estimation ability of the proposed models.
- The correlation coefficient (R^2) between the prediction and experimental data in SEM is higher than that of WFM. Compared to WFM, improving the R^2 value in SEM is more significant than previous relationships. Compared to the basic Kriging models, the use of K-Means and U-function to generate the combined Kriging models in SEM leads to better R^2 values. But in WFM, the use of K-Means reduces the R^2 parameter compared to the basic Kriging models and the use of the U-function.
- The mean error of the proposed Kriging models in WFM is in the range of 8.8–19.5 and is less than the previously available relationships (21%–78.6%). However, in SEM, different combined models with 10% of the data have a higher mean error value than previous relationships. The lowest average errors in determining the fracture energy among all the proposed Kriging models in SEM and WFM belong to K4-50 and U-50, respectively.
- G_F/G_f values of Rand-10, Rand-50, K2-30, and K4-30 models are more than 2.5. However, this parameter is in the range of 2–2.5 for other models. Selecting a smaller and larger number of training data in the proposed Kriging models makes the G_F/G_f values to be close to the lower limit (2) and the upper limit (2.5), respectively.
- Compared to the neural network method with less training data, the use of the Kriging method has increased the accuracy of the concrete fracture energy prediction results.

Author statement

Iman Afshoon: Resources, Writing - Original Draft, Data curation, Writing- Original draft preparation, Software.

Mahmoud Miri: Conceptualization, Methodology, Investigation, Reviewing and Editing, Supervision, Project administration, funding acquisition.

Seyed Roohollah Mousavi: Resources, Writing - Original Draft, Data curation, Writing- Original draft preparation, Software.

Declaration of competing interest

The authors declare that they have no known competing financial interests or personal relationships that could have appeared to influence the work reported in this paper.

Table 9
Results of G_F/G_f for different models.

G_F/G_f Ratio	kriging models												
	Rand-10	Rand-30	Rand-50	U-base	U-10	U-30	U-50	K2-10	K2-30	K2-50	K4-10	K4-30	K4-50
Min	1.56	1.01	1.20	0.94	0.98	1.06	0.93	1.02	1.18	1.28	1.16	1.05	0.88
Max	5.66	3.81	3.70	3.92	3.89	4.07	3.98	4.02	3.59	3.72	3.76	3.88	3.66
Average	3.05	2.37	2.52	2.09	2.22	2.43	2.39	2.47	2.51	2.50	2.30	2.70	2.48

References

[1] M. Janssen, J. Zuidema, R. Wanhill, Fracture Mechanics VSSD, 2006.
[2] S. Xu, H.W. Reinhardt, Crack extension resistance and fracture properties of quasi-brittle softening materials like concrete based on the complete process of fracture, Int. J. Fract. 92 (1) (1998) 71–99.
[3] R.K. Choubey, S. Kumar, M.C. Rao, Modeling of fracture parameters for crack propagation in recycled aggregate concrete, Construct. Build. Mater. 106 (2016) 168–178.
[4] M. Ghasemi, M.R. Ghasemi, S.R. Mousavi, Investigating the effects of maximum aggregate size on self-compacting steel fiber reinforced concrete fracture parameters, Construct. Build. Mater. 162 (2018) 674–682.
[5] A.S. Rao, G.A. Rao, Fracture mechanics of fiber reinforced concrete: an overview, International Journal of Engineering Innovations and Research 3 (4) (2014) 517.
[6] Z.P. Bazant, J.-K. Kim, P.A. Pfeiffer, Determination of fracture properties from size effect tests, J. Struct. Eng. ASCE 112 (1986) 289–307.
[7] J. Safari, M. Mirzaei, H. Rooholamini, A. Hassani, Effect of rice husk ash and macro-synthetic fibre on the properties of self-compacting concrete, Construct. Build. Mater. 175 (2018) 371–380.
[8] Z. Bažant, B. Oh, Crack band theory for fracture of concrete, Mater. Struct. 16 (1983) 155–177.
[9] P. Nallathambi, B.L. Karihaloo, Determination of specimen-size independent fracture toughness of plain concrete, Mag. Concr. Res. 38 (135) (1986) 67–76.
[10] Y.S. Jenq, S.P. Shah, Two parameter fracture model for concrete, J. Eng. Mech. ASCE 111 (1985) 1227–1241.
[11] G. Cusatis, E.A. Schauffert, Cohesive crack analysis of size effect, Eng. Fract. Mech. 76 (2009) 2163–2173.
[12] M. Elices, C. Rocco, C. Roselló, Cohesive crack modeling of a simple concrete: experimental and numerical results, Eng. Fract. Mech. 76 (2009) 1398–1410.
[13] S. Xu, X. Zhang, Determination of fracture parameters for crack propagation in concrete using an energy approach, Eng. Fract. Mech. 75 (2008) 4292–4308.
[14] S. Kumar, S.V. Barai, Influence of specimen geometry and size-effect on the KR curve based on the cohesive stress in concrete, Int. J. Fract. 152 (2008) 127–148.
[15] S. Kumar, S.V. Barai, Weight function approach for determining crack extension resistance based on the cohesive stress distribution in concrete, Eng. Fract. Mech. 76 (2009) 1131–1148.
[16] S. Hu, Z. Mi, J. Lu, Effect of crack-depth ratio on double-K fracture parameters of reinforced concrete, Appl. Mech. Mater. 226–228 (2012) 937–941.
[17] R. Ince, Determination of the fracture parameters of the double-K model using weight functions of split-tension specimens, Eng. Fract. Mech. 96 (2012) 416–432.
[18] K. Yu, Z. Lu, Determining residual double-K fracture toughness of post fire concrete using analytical and weight function method, Mater. Struct 47 (2013) 839–852.
[19] S. Kumar, S.R. Pandey, A.K.L. Srivastava, Determination of double-K fracture parameters of concrete using peak load method, Eng. Fract. Mech. 131 (2014) 471–484.
[20] H. Cifuentes, B.L. Karihaloo, Determination of size-independent specific fracture energy of normal- and high-strength self-compacting concrete from wedge splitting tests, Construct. Build. Mater. 48 (2013) 548–553.
[21] K. Duan, X. Hu, F.H. Wittmann, Boundary effect on concrete fracture and non-constant fracture energy distribution, Eng. Fract. Mech. 70 (2003) 2257–2268.
[22] T.C.S. Rilem, Determination of the fracture energy of mortar and concrete by means of three-point bend tests on notched beames, Mater. Struct. 18 (1985) 285–290.
[23] I.M. Nikbin, S. Rahimi, H. Allahyari, A new empirical formula for prediction of fracture energy of concrete based on the artificial neural network, Eng. Fract. Mech. 186 (2017) 466–482.
[24] Z.P. Bazant, M.T. Kazemi, Determination of fracture energy, process zone length and brittleness number from size effect, with application to rock and concrete, IJFr 44 (1990) 111–131.
[25] R.A. Einsfeld, M.S.L. Velasco, Fracture parameters for high-performance concrete, Cement Concr. Res. 36 (2006) 576–583.
[26] M. Beygi, J. Berenjian, O. Omran, A.S. Nik, I.M. Nikbin, An experimental survey on combined effects of fibers and nano-silica on the mechanical, rheological, and durability properties of self-compacting concrete, Mater. Des. 50 (2013) 1019–1029.
[27] M. Ghasemi, M.R. Ghasemi, S.R. Mousavi, Studying the fracture parameters and size effect of steel fiber-reinforced self-compacting concrete, Construct. Build. Mater. 201 (2019) 447–460.
[28] M.T. Kazemi, H. Golsorkhtabar, M.H.A. Beygi, M. Gholamitabar, Fracture properties of steel fiber reinforced high strength concrete using work of fracture and size effect methods, Construct. Build. Mater. 142 (2017) 482–489.
[29] Aref Shafiei Dastgerdi, J. Robert, b Peterman, Kyle Riding c, B. Terry Beck, Effect of concrete mixture components, proportioning, and compressive strength on fracture parameters, Construct. Build. Mater. 206 (2019) 179–192.
[30] F.H. Wittmann, P.E. Roelfstra, H. Mihashi, Y.-Y. Huang, X.-H. Zhang, et al., Influence of age of loading, water–cement ratio and rate of loading on fracture energy of concrete, Mater. Struct. 20 (2) (1987) 103–110.
[31] A. Carpinteri, R. Brighenti, Fracture behaviour of plain and fiber-reinforced concrete with different water content under mixed mode loading, Mater. Des. 31 (4) (2010) 2032–2042.
[32] P. Nallathambi, B. Karihaloo, B. Heaton, Effect of specimen and crack sizes, water/cement ratio and coarse aggregate texture upon fracture toughness of concrete, Mag. Concr. Res. 36 (129) (1984) 227–236.
[33] S. Mindess, F. Young, D. Darwin, Concrete, second ed., Prentice Hall, Upper Saddle River (NJ), 2003.
[34] D.V. Phillips, Z. Binsheng, Direct tension tests on notched and un-notched plain concrete specimens, Mag. Concr. Res. 45 (162) (1993) 25–35.
[35] Z. Zhao, S.H. Kwon, S.P. Shah, Effect of specimen size on fracture energy and softening curve of concrete: Part I. Experiments and fracture energy, Cement Concr. Res. 38 (2008) 1049–1060.
[36] R. Ince, K.E. Alyamac, Determination of fracture parameters of concrete based on water–cement ratio, Indian J. Eng. Mater. Sci. 15 (2008) 14–22.
[37] B. Chen, J. Liu, Effect of aggregate on the fracture behaviour of high strength concrete, Construct. Build. Mater. 18 (2004) 585–590.
[38] J. Brown, C. Pomeroy, Fracture toughness of cement paste and mortars, Cement Concr. Res. 3 (4) (1973) 475–480.
[39] N. Isu, S. Teramura, H. Ishida, Influence of quartz particle size on the chemical and mechanical properties of autoclaved aerated concrete (II) fracture toughness, strength and micropore, Cement Concr. Res. 25 (2) (1995) 249–254.
[40] T. Dittmer, H. Beushausen, The effect of coarse aggregate content and size on the age at cracking of bonded concrete overlays subjected to restrained deformation, Construct. Build. Mater. 69 (2014) 73–82.
[41] M. Elices, C.G. Rocco, Effect of aggregate size on the fracture and mechanical properties of a simple concrete, Eng. Fract. Mech. 75 (2008) 3839–3851.
[42] G. Appa Rao, B.K. Raghu Prasad, Fracture energy and softening behavior of high-strength concrete, Cement Concr. Res. 32 (2002) 247–252.
[43] M.H.A. Beygi, M.T. Kazemi, J. Vaseghi Amiri, I.M. Nikbin, S. Rabbanifar, E. Rahmani, Evaluation of the effect of maximum aggregate size on fracture behavior of self-compacting concrete, Construct. Build. Mater. 55 (2014) 202–211.
[44] P.E. Petersson, Fracture energy of concrete: practical performance and experimental results, Cement Concr. Res. 10 (1) (1980) 91–101.
[45] M. Neshat, et al., A comparative study on ANFIS and fuzzy expert system models for concrete mix design, Int. J. Comput. Sci. Issues 8 (3) (2011) 196–210.
[46] M. Nehdi, M. Bassuoni, Fuzzy logic approach for estimating durability of concrete, Proc. Ins. Civ. Eng.-Constr. Mater. 162 (2) (2009) 81–92.
[47] Z.P. Bazant, P. Pfeiffer, Determination of fracture energy from size effect and brittleness number, ACI Mater. J. 84 (6) (1987) 463–480.
[48] J. Vahedi, M.R. Ghasemi, M. Miri, An adaptive divergence-based method for structural reliability analysis via multiple Kriging models, Appl. Math. Model. 62 (2018) 542–561.
[49] Y. Moodi, S. R Mousavi, A. Ghavidel, M.R. Sohrabi, M. Rashki, Using Response Surface Methodology and providing a modified model using whale algorithm for estimating the compressive strength of columns confined with FRP sheets, Construct. Build. Mater. 183 (2018) 163–170.
[50] S. Khalilpour, E. BaniAsad, M. Dehestani, A review on concrete fracture energy and effective parameters, Cement Concr. Res. 120 (2019) 294–321.
[51] R. Ince, Prediction of fracture parameters of concrete by artificial neural networks, Eng. Fract. Mech. 71 (2004) 2143–2159.
[52] Y. Yan, Q. Ren, N. Xia, L. Shen, J. Gu, Artificial neural network approach to predict the fracture parameters of the size effect model for concrete, Fatig. Fract. Eng. Mater. Struct. 38 (2015) 1347–1358.
[53] J.Y. Kang, B.I. Choi, H.J. Lee, Application of artificial neural network for predicting plain strain fracture toughness using tensile test results, Fatig. Fract. Eng. Mater. Struct. 29 (2006) 321–329.
[54] R. Ince, Determination of concrete fracture parameters based on two-parameter and size effect models using split-tension cubes, Eng. Fract. Mech. 77 (2010) 2233–2250.
[55] J. Guana, C. Lia, J. Wang, L. Qingc, Z. Songa, Z. Liua, Determination of fracture parameter and prediction of structural fracture using various concrete specimen types, Theor. Appl. Math. Model. 100 (2019) 114–127.
[56] Z.P. Bazant, E. Becq-Giraudon, Statistical prediction of fracture parameters of concrete and implications for choice of testing standard, Cement Concr. Res. 32 (2002) 529–556.
[57] Ceb-Fip, CEB-FIP model code (1990) 460, https://doi.org/10.1680/ceb-fipmc1990.35430, 1990.
[58] CEB-FIP Model Code. Fib Model Code for Concrete Structures 2010, Doc Competence Cent Siegmar Kästl eK, Ger, 2010.

[59] Japan Society of Civil Engineers, Standard specifications for concrete structures (2007). "Design". 2007; 15:1–503.
[60] D.R. Jones, M. Schonlau, J. William, Efficient global optimization of expensive black-box functions, J. Global Optim. 13 (1998) 455–492.
[61] J. Sacks, W.J. Welch, T.J. Mitchell, H.P. Wynn, Design and analysis of computer experiments, Stat. Sci. 4 (1989) 409–423.
[62] F.A. Viana, T.W. Simpson, V. Balabanov, V. Toropov, Special section on multidisciplinary design optimization: metamodeling in multidisciplinary design optimization: how far have we really come? AIAA J. 52 (4) (2014) 670–690.
[63] W.Y. Yun, Z.Z. Lu, X. Jiang, Ak-SYSi: An improved adaptive Kriging model for system reliability analysis with multiple failure modes by refined U learning function, Struct. Multidiscip. Optim 59 (2019) 263–278.
[64] Y.C. Zhou, Z.Z. Lu, K. Cheng, W.Y. Yun, A Bayesian Monte Carlo-based method for efficient computation of global sensitivity indices, Mech. Syst. Signal Process. 117 (5) (2019) 498–516.
[65] G. Matheron, The intrinsic random functions and their applications, Adv. Appl. Probab. 5 (3) (1973) 439–468.
[66] E.I. Flores, F.A. DiazDelaO, M.I. Friswell, et al., A computational multi-scale approach for the stochastic mechanical response of foam filled honeycomb cores, Compos. Struct. 94 (2012) 1861–1870.
[67] C. Ling, Z. Lu, B. Sun, M. Wang. An Efficient Method Combining Active Learning Kriging and Monte Carlo Simulation for Profust Failure Probability. Fuzzy Sets and Systems.
[68] L.G. Zhang, Z.Z. Lu, P. Wang, Efficient structural reliability analysis method based on advanced Kriging model, Appl. Math. Model. 39 (2015) 781–793.
[69] B. Sudret, Meta-models for structural reliability and uncertainty quantification, arXiv preprint arXiv 1 (2012), 1203.2062.
[70] B.J. Bichon, M.S. Eldred, L.P. Swiler, S. Mahadevan, J.M. McFarland, Efficient global reliability analysis for nonlinear implicit performance functions, AIAA J. 46 (2008) 2459–2468.
[71] B. Echard, N. Gayton, M. Lemaire Ak-Mcs, An active learning reliability method combining Kriging and Monte Carlo simulation, Struct. Saf. 33 (2) (2011) 145–154.
[72] D.D. Cox, S. John, Statistical method for global optimization, in: M.N. Alexandrov, M.Y. Hussaini (Eds.), Multidisciplinary Design Optimization: State-Of-The-Art, Siam, Philadelphia, 1997, pp. 315–329.
[73] X. Huang, Y. Ye, H. Guo, Y. Cai, H. Zhang, Y. Li, DSKmeans: a new kmeans-type approach to discriminative subspace Clustering, Knowl. Base Syst. 70 (2014) 293–300.
[74] M. Anisur Rahman, M. Zahidul Islam, Application of a density based clustering technique on biomedical datasets, Appl. Soft. Compu. Jour. 73 (2018) 623–634.
[75] S. Zahra, M. r Ali Ghazanfar, A. Khalid, M. Awais Azam, U. Naeem, A. Prugel-Bennett, Novel centroid selection approaches for KMeans clustering based recommender systems, Inf. Sci. 320 (2015) 156–189.
[76] X. Wang, H.A. Saifullah, H. Nishikawa, K. Nakarai, Effect of water–cement ratio, aggregate type, and curing temperature on the fracture energy of concrete, Construct. Build. Mater. 259 (2020) 119646.
[77] D. Darwin, S. Barham, Rozalija Kozul, Shuguang Luan, Fracture energy of high-strength concrete, ACI Mater. J. 98 (5) (2001) 410–417.
[78] R. Kozul, D. Darwin, Effects of Aggregate Type, Size, and Content on Concrete Strength and Fracture Energy, University of Kansas Center for Research Inc, 1997.
[79] A. Yan, K.R. Wu, D. Zhang, W. Yao, Effect of fracture path on the fracture energy of high-strength concrete, Cement Concr. Res. 31 (2001) 1601–1606.
[80] J.T. Yu, K.Q. Yu, Z.D. Lu, Residual fracture properties of concrete subjected to elevated temperature, Mater. Struct. 45 (2012) 1155–1165.
[81] J. Planas, M. Elices, G.V. Guinea, Measurement of the fracture energy using three-point bend tests: part 2—influence of bulk energy dissipation, Mater. Struct. 25 (1992) 305–312.